JOURNAL OF SPACECRAFT AND ROCKETS
Vol. 38, No. 2, March–April 2001

Thermal Load Effects on Precision Membranes

C. H. Jenkins*
South Dakota School of Mines and Technology, Rapid City, South Dakota 57701
and
S. M. Faisal†
Federal Mogul Corporation, Plymouth, Michigan 48170

The potential for placing large, ultralightweight precision reflectors in space is currently being investigated through use of membrane structures. Their capacity for reducing launch mass and stowed volume is being exploited. However, on-orbit performance will require an understanding of the effects of thermal loads on reflector surface precision. Thermal load effects cut both ways, and selective heating of the reflector may someday be used to effect desirable changes in the surface profile. Both theoretical and experimental analyses are provided of an inflated membrane reflector with a thermal load acting on its surface. A goal was to compare temperature-induced changes in shape with the results obtained for enforced boundary displacements along the entire rim, which has previously been shown to be an effective control strategy. The Hencky/Campbell problem is solved numerically (Hencky, H., "Uber den Spannungszustand in Kreisrunde Platten," *Z. Mathematics and Physics*, Vol. 63, 1915, pp. 311–317; Campbell, J. D., "On the Theory of Initially Tensioned Circular Membranes Subjected to Uniform Pressure," *Quarterly Journal of Mechanics and Applied Mathematics*, Vol. 9, 1956, pp. 84–93), but with a thermal strain imposed. The nonlinear finite element code ABAQUS is then used for comparison. The model was studied for different temperature profiles, varying both in temperature magnitude and spatial extent. Finally, a preliminary experiment is performed, using infrared thermography to measure the membrane surface temperature, and these results are compared to the theoretical models.

Nomenclature

a	=	radius of circular membrane
D	=	bending rigidity
E	=	elastic modulus
h	=	membrane thickness
M	=	moment resultant
N	=	stress resultant
p	=	pressure
q	=	nondimensional load parameter
r	=	radial coordinate
T	=	temperature
u	=	radial displacement
w	=	axial or z displacement
x	=	spatial coordinate
y	=	spatial coordinate
z	=	spatial coordinate
α	=	coefficient of thermal expansion
ε	=	radial strain
ν	=	Poisson's ratio
ϕ	=	stress function

Subscripts

O	=	mechanical prestrain
T	=	thermal

Introduction

THERE currently exists renewed interest in application of membrane structures in space. With increased pressure to reduce costs associated with design, fabrication, and launch of space structures, the Department of Defense (DOD) and NASA are taking a new look at space-based membrane structures. Applications include lunar and planetary habitats, rf reflectors and waveguides, optical and infrared (IR) imaging, solar concentrators for solar power and propulsion, sun shades, and solar sails. For many of these applications, particularly those involved with communications, imaging, power, and propulsion, accurate maintenance of the membrane surface shape is critical. Ideally, surface accuracy ranges from a few percent of wavelength for low-frequency applications to a fraction of a percent of wavelength for visible wavelengths should apply. However, the likelihood of achieving such tolerances on membrane surfaces by purely passive means is small,[1,2] and active control of the surface and/or adaptive wave front correction are indicated.

The purpose of this paper is to report results of a study on thermal load effects on precision membranes. The problem of the inflation of an initially plane, thermoelastic circular membrane, with deformations limited to those that admit only small strains but moderately large rotations is reviewed (see Jenkins and Leonard[3] and Jenkins[4] for additional details). Next, we discuss use of finite element analysis (FEA) to demonstrate the effects of thermal loads applied to the model, as well as boundary (rim) displacements, on the deformed shape of an inflated circular membrane. Both actions (boundary displacements and thermal loads) may be considered as active control strategies to achieve a parabolic profile, that is, methods to reduce the deviation of the surface shape from a reference paraboloid (the figure error). The FEA model was studied for different temperature profiles, varying both in temperature value and spatial extent. The FEA considered 1) a uniform boundary displacement only, 2) a temperature profile only, and 3) a temperature profile along with uniform boundary displacements. Theoretical calculations were performed to compare with FEA results. Finally, an experiment was conducted with temperature applied to a membrane reflector model, and the results compared to the FEA.

Elastic Deformations of Circular Membrane

Hencky[5] provided the first (numerical) solution to the membrane form of the von Kármán plate equations. A modern treatment has been given recently by Fichter[6] and Wilkes.[7] Campbell[8] reconsidered the Hencky problem, except the boundary conditions in the reference configuration allow a purely radial displacement to provide for a mechanical prestress. Wilkes[7] has generalized Campbell's solution,[8] and we follow Wilkes's[7] numerical procedure for our results (see Ref. 9).

Received 5 May 1999; revision received 1 August 2000; accepted for publication 8 January 2001. Copyright © 2001 by the American Institute of Aeronautics and Astronautics, Inc. All rights reserved.

*Professor, Mechanical Engineering Department, and Director, Compliant Structures Laboratory, 501 E. Saint Joseph Street. Member AIAA.
†CAD/CAE Application Analyst, Technical Center, 47001 Port Street.

Table 1 ABAQUS model data

Model[a]	Young's Modulus E, GPa (ksi)	Thickness h, mm (in.)	Coefficient of thermal expansion α, mm/mm/°C (in./in./°F)	Poisson's ratio, ν	f-number	Radius a, mm (in.)
1	1.38 (200)	0.032 (0.00125)	19E−6 (35E−6)	0.4	2.27	218 (8.6)
2	4.83 (700)	0.1 (0.004)	19E−6 (35E−6)	0.4	1.95	216 (8.5)

[a]Model 1 is a somewhat arbitrary configuration, and model 2 represents the physical experiment.

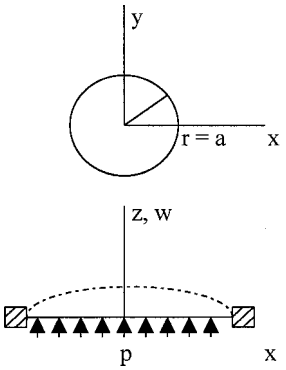

Fig. 1 Definition: top plan view and bottom meridional section.

Thermoelastic Deformations of Circular Membrane

The von Kármán plate equations in axisymmetric form can be generalized to account for the thermoelastic strain[10]:

$$D\left(\frac{\mathrm{d}^2}{\mathrm{d}r^2}+\frac{1}{r}\right)^2 w-\frac{h}{r}\frac{\mathrm{d}}{\mathrm{d}r}\left(\frac{\mathrm{d}\phi}{\mathrm{d}r}\frac{\mathrm{d}w}{\mathrm{d}r}\right)=p+\nabla^2 M_T \tag{1}$$

$$r\frac{\mathrm{d}}{\mathrm{d}r}\left(\frac{\mathrm{d}^2\phi}{\mathrm{d}r^2}+\frac{1}{r}\frac{\mathrm{d}\phi}{\mathrm{d}r}\right)+\frac{E}{2}\left(\frac{\mathrm{d}w}{\mathrm{d}r}\right)^2+\frac{1-\nu}{h}\nabla^2(N_T)=0 \tag{2}$$

where $D=Eh^3/12(1-\nu^2)$ is the bending rigidity and M_T is the thermal moment resultant (Fig. 1). N_T is the thermally induced in-plane (membrane) stress resultant defined by

$$N_T=\frac{1}{1-\nu}\int_{-h/2}^{h/2} E\alpha T(r)\,\mathrm{d}z \tag{3}$$

In our study, we assume that α is a constant and that temperature varies only in the radial direction, that is, $T=T(r)$, and hence, $\nabla^2 M_T=0$ (because temperature does not vary through the thickness and no thermal couple exits). Thus, the thermal stress resultant term, after integrating from Eq. (3), yields

$$N_T=[Eh/(1-\nu)]\alpha T(r) \tag{4}$$

Substituting the value of N_T from Eq. (4) to Eq. (2) yields

$$r\frac{\mathrm{d}}{\mathrm{d}r}\left(\frac{\mathrm{d}^2\phi}{\mathrm{d}r^2}+\frac{1}{r}\frac{\mathrm{d}\phi}{\mathrm{d}r}\right)=-\frac{E}{2}\left(\frac{\mathrm{d}w}{\mathrm{d}r}\right)^2-E\alpha\nabla^2 T(r) \tag{5}$$

From the preceding equation it can be seen that the thermal stress resultant can be considered to induce a prestress (or prestrain) to the membrane, which corresponds to Campbell's[8] mechanical prestress (prestrain).

In this study, the total thermoelastic strain due to heating and cooling was considered as a prestrain to calculate the deformed membrane profile (meridional curve) theoretically. The curve was determined following Wilkes[7] (see Ref. 9), taking the strain as positive for cooling and negative for heating.

For the three temperature distributions considered in the present work, uniform, linear, and parabolic profiles, and to be useful in the theoretical model, the total prestrain $\langle\varepsilon\rangle$ was calculated by averaging the thermal strain function over the radius:

$$\langle\varepsilon\rangle=\frac{1}{a}\int_0^a \alpha T(r)\,\mathrm{d}r+\varepsilon_0 \tag{6}$$

where $T(r)$ is the temperature distribution in the membrane. In Eq. (6), ε_0 is the mechanical prestrain due to the displacement boundary condition and was calculated according to the following equation:

$$u=\int_0^a \varepsilon(r)\,\mathrm{d}r=\varepsilon_0 a \tag{7}$$

The average prestrain found from Eq. (6) was used in the theoretical model, which was then compared to the FEA model.

FEA

It has been observed in inflatable reflectors that their service shape deviates from the desired parabolic profile as a function of position on the reflector, inflation pressure, material properties, manufacturing effects, etc. When the difference between the actual profile and desired parabolic shape (the figure error) is plotted, a characteristic W shape or W curve results. If the initially plane disk does not have an inflated shape that is a paraboloid, then questions naturally arise then about how one might manipulate the shape to approach becoming parabolic.

The study reported here considered two possible procedures to control the shape: 1) by enforced boundary displacement at the rim[11] and 2) by a controlled heating of the surface. FEA (the nonlinear code ABAQUS) was used to verify both the experimental and theoretical results. The two different models used are listed in Table 1.

ABAQUS Model for Temperature Load Simulation (Table 1, Model 1)

The model consisted of 48 second-order membrane elements and 157 nodes. All of the boundary nodes were fixed in the x, y, and z directions. Linear elastic properties were assumed in the model, as shown in Table 1. The pressure used was 0.14 kPa (0.02 psi), which resulted in $f=2.27$ where f-number is the ratio of focal length to aperture diameter $2a$.

The temperature was considered a static loading with step distribution, the axisymmetric step change occurring at two different radial positions, $r=114$ and 76.2 mm (4.50 and 3.0 in.), as shown in Fig. 2. Constant temperatures of 4.44 and 10°C (40 and 50°F) were specified on the model over a circular region defined by a radius of $r=114$ mm (4.50 in.) or $r=76.3$ mm (3.0 in.), while all other nodes were maintained at 0°C temperature (Table 2 and Fig. 2).

The resulting FEA z-displacement profiles (meridian curves) were compared to a reference parabola. The intersection points between the meridian curve and the coordinate axes, that is, at the maximum z deflection w_0 or the apex of the membrane surface and at the radius a of the surface (Fig. 1), can be used to define a reference parabolic curve w_p, according to the equation $w_p=w_0(1-r^2/a^2)$. The W curve was obtained from the difference between this parabola and the deformed surface z displacement, w.

A static analysis was conducted that resulted in a maximum deflection of 12.2 mm (0.482 in.) and von Mises stress of 2410–3310 kPa (350–480 psi) for the 4.44°C temperature case. After the temperature was applied, a center deflection of 15.3 mm (0.604 in.) was achieved at pressure 0.14 kPa (0.02 psi), but because the comparison should be done for the same f-number, the pressure was

Table 2 Thermal analysis results and description

Case	Temperature,[a] °C	Temperature region[a] radius, mm	Minimum rms error, mm: Boundary displacement at 1.27 mm only	Minimum rms error, mm: Temperature only	Minimum rms error, mm: Temperature plus displacement at 1.27 mm
1a	4.44	$0 \le r \le 114$	0.0940	0.0889	0.0340
1b	10	$0 \le r \le 114$	0.0940	0.0370	0.0180
2a	4.44	$0 \le r \le 76.2$	0.0940	0.0910	0.0381
2b	10	$0 \le r \le 76.2$	0.0940	0.0810	0.0279
3a	4.44	$114 \le r \le 218$	0.0940	0.685	0.160
3b	10	$114 \le r \le 218$	0.0940	0.787	0.165

[a]See Fig. 2 for schematic of temperature profiles.

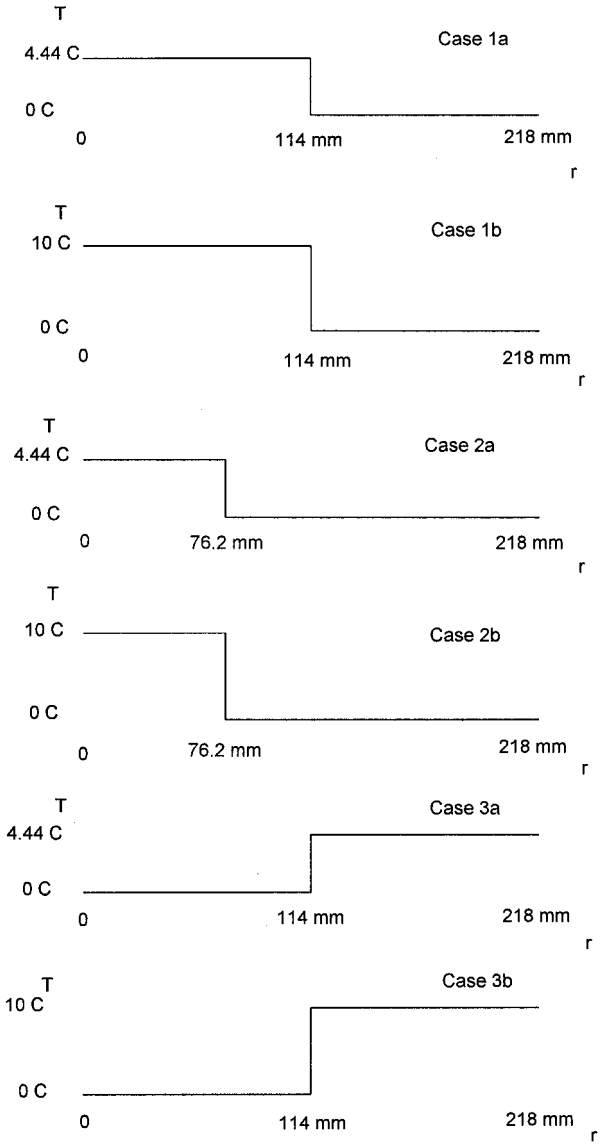

Fig. 2 Temperature distributions, which are step changes in temperature, occurring at two different radial positions.

adjusted to maintain $f = 2.27$. (A change in f-number can itself induce changes in surface figure.)

Imposed outward radial displacements of 1.27 mm (0.05 in.) along the entire rim were also applied, which resulted in a decrease in the center deflection. The pressure was again adjusted in order to maintain constant f-number.

ABAQUS Model of the Thermal Experiment (Table 1, Model 2)

The FEA model of the thermal experiment attempted to replicate the experimental configuration as closely as possible (Fig. 3). The upper surface of the balloon was modeled with symmetry boundary conditions as before, and the radial Kevlar® tie lines were modeled as well. The model consisted of 56 second-order membrane elements and 239 nodes. The tie lines were modeled as beam elements with circular cross section and appropriate Young's modulus (see Ref. 9). Linear elastic properties were assumed in this model as well (Table 1).

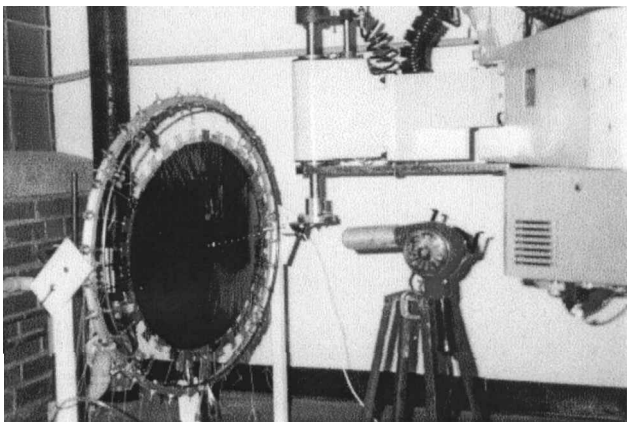

Fig. 3 Experimental setup: left, membrane (Mylar balloon) and radial ties to the support fixture; center, capacitance displacement sensor on robot arm; and right, air gun heat source.

Experimental Analysis

An experiment was conducted to verify the FEA models described. Available funds limited the sophistication of the experiment (the required noncontact heating, thermal, and displacement measurement are extremely challenging tasks); however, results gathered confirm the model and provide a foundation for future experimental work. The experimental setup consisted of a mylar balloon and subsystems (Fig. 3), of which brief details are provided next. (Complete details of the experiment are given in Ref. 9, including experimental uncertainty, estimated to be about 5% of the measured temperature and less than 1% for measured displacements.)

Temperature Generation and Measurement System

The balloon was heated with a hot air gun, which was mounted on a stand facing normal to the balloon surface at a distance of approximately 30.5 cm (1 ft). The pressure inside the balloon was kept constant during this process by monitoring with a mercury manometer.

To measure the temperature along a meridian, a Video Therm 2000 IR camera was used. The model 2000 is a portable thermal imaging system, which utilizes a solid state uncooled focal plane array. The detector is manufactured by Raytheon TI Systems (formally Texas Instruments) and is composed of 320 × 240 (76,800) individual IR detectors.

Robot Displacement Measurement System

The surface profile mapping system consisted of an industrial robot, controlled by a personal computer, which held a capacitance displacement sensor. The robotic mechanism was used under

closed-loop control, with two degrees of freedom that are accurate to 0.01 mm (0.0004 in.).

The heart of the measurement system is the capacitance displacement sensor (Capacitec Model HPT-75). This cylindrically shaped noncontact sensor, of 1.9-mm (0.075-in.) core diameter, acts as one-half of a capacitor, while the membrane surface (conductive Mylar®) acts as the other half. The sensor returns a voltage proportional to the air gap between itself and the Mylar surface. This measurement, coupled with the knowledge of the arm position, gives a direct and accurate indication of the surface profile.

Results and Discussion

Comparison of FEA and Theoretical Results: General

The theoretical models were compared with FEA models for temperature loading and boundary displacements. Theoretical models were calculated for the nondimensional load parameter $q = pa/Eh = 0.0007$, using a pressure of 0.14 kPa and other parameter values as shown in Table 1.

Effects of Enforced Boundary Displacements

Figure 4 shows the comparison of theoretical and FEA z-displacement results, with and without a 1.27-mm (0.05-in.) uniform boundary displacement, at uniform temperature of 0°C (FEA model 1). In Fig. 4, the following cases are shown: BD1a is a reference parabola, FEA with no boundary displacement; BD1b is a reference parabola, theoretical model with no boundary displacement; BD2a is a reference parabola, FEA with 1.27-mm (0.05-in.) uniform boundary displacement; and BD2a is a reference parabola, theoretical model with 1.27-mm (0.05-in.) uniform boundary displacement. The mechanical prestrain was calculated from the boundary displacement of 1.27 mm using Eq. (7), or $\varepsilon_0 = 1.27/218 = 0.006$. Good agreement is seen between the two models.

Effects of Temperature Distribution

For the uniform temperature case, the total prestrain calculated from Eq. (6) was $\varepsilon = \alpha T + \varepsilon_0$. The temperature function used for linear temperature profile was $T(r) = 4.65r - 40$, whereas for parabolic temperature profile $T(r) = T_0[1 - (r/a)^2]$.

Figure 5 shows the comparison of theoretical and FEA z-displacement results without boundary displacements and with various uniform temperatures applied (FEA model 1). In Fig. 5, the following cases are shown: TP1a is a reference parabola, FEA with uniform temperature of 0°C; TP1b is a reference parabola, theoretical model with uniform temperature of 0°C; TP2a is a reference parabola, FEA with uniform temperature of 4.44°C; TP2b is a reference parabola, theoretical model with uniform temperature of 4.44°C; TP3a is a reference parabola, FEA with uniform temperature of −4.44°C; and TP3b is a reference parabola, theoretical model with uniform temperature of −4.44°C. Good agreement is again seen between the two models. (The results for step temperature distribution are not shown, but for the linear distribution the models deviate by 2.3%, whereas for the parabolic distribution the deviation is 5%.)

For any given extent of the heated region, the magnitude and sign of the temperature difference is important. In Fig. 5, deviation from parabolic is improved with the −4.44°C uniform temperature, but made worse with the +4.44°C uniform temperature.

Additional results are shown in Table 2, using the step temperature profiles shown in Fig. 2. For example, for the cases 1b and 2b, where a temperature difference of 10°C is specified in the respective heated inner circular regions (and 0°C elsewhere), the membrane surface deviation reduced compared to heating the same region at the lower temperature of 4.44°C (cases 1a and 1b, respectively). (However, at larger temperature differences, the deviations can actually increase.[9])

Effects of Boundary Displacement and Temperature Distribution

With a temperature difference of 10°C in case 2b, the deviation was comparable to the case with boundary displacements only (0.0810 vs. 0.0940 mm, respectively). However, combining boundary displacements and temperature together results in a rms value of 0.0279 mm, reducing the deviation below either method applied separately (see Table 2).

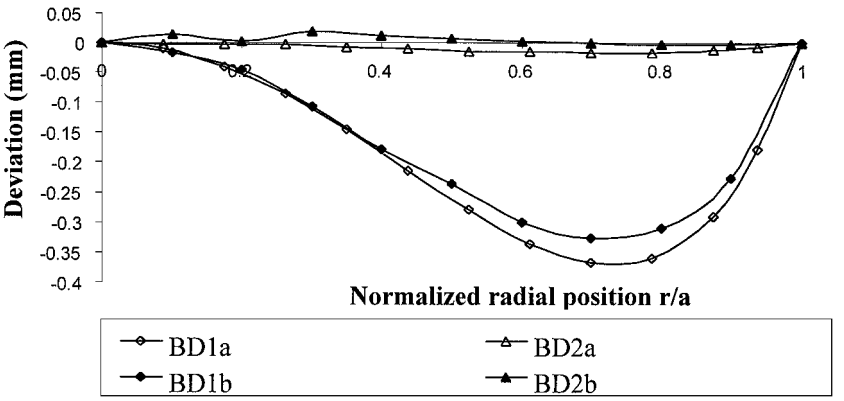

Fig. 4 Difference of theoretical and FEA z displacements (W curve), with and without boundary displacements, for $q = 0.0007$ and a uniform temperature of 0°C.

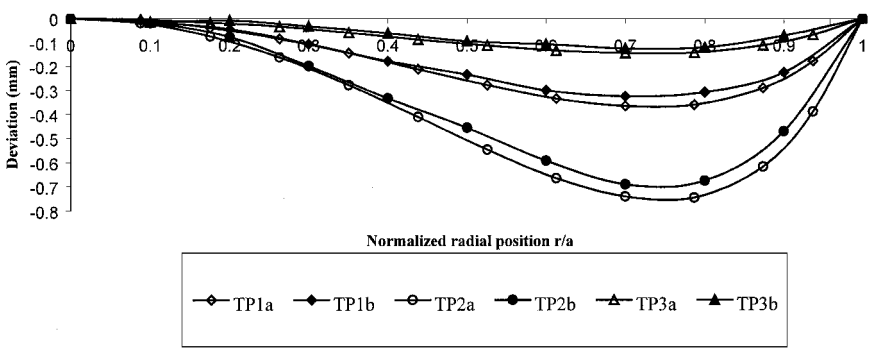

Fig. 5 Difference of theoretical and FEA z displacements (W curve), without boundary displacements, for $q = 0.0007$ and various uniform temperatures applied.

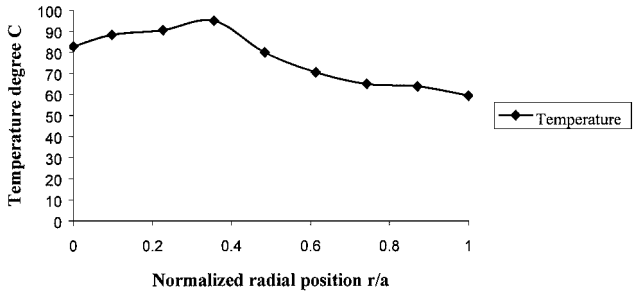

Fig. 6 Temperature profile measured on the balloon surface during the experiment.

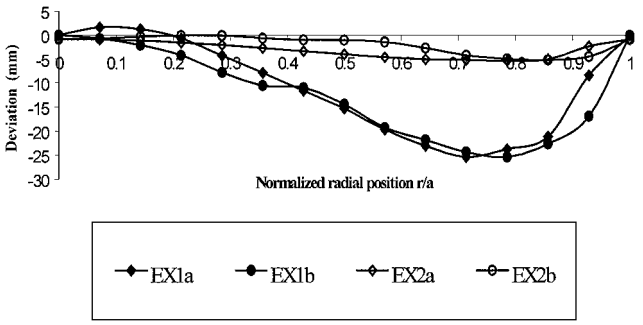

Fig. 7 Difference of experimental and FEA z displacements, without boundary displacements, for $q = 0.0013$ and various temperature profiles.

In results similar to those shown in Fig. 5 and discussed earlier, when the outer annular region was heated relative to the center (cases 3a and 3b), the deviation from parabolic worsened. However, even in these cases, when boundary displacements were combined with the outer annulus heating, the resulting deviations were reduced significantly.

Effects of Temperature Gradient Determined Experimentally

The temperature profile obtained during the experiment is shown in Fig. 6. The experimental setup was then modeled as closely as possible in ABAQUS. The model was tuned to match the experimentally measured center deflection. Figure 7 shows the comparison between FEA and experiment. The following cases are shown in Fig. 7: EX1a is a reference parabola, FEA with experimental temperature profile of Fig. 6; EX1b is a reference parabola, experimental (temperature profile of Fig. 6); EX2a is a reference parabola, FEA with uniform room temperature; and EX2b is a reference parabola, experimental (at uniform room temperature).

Before the thermal load was applied, the experimental rms error (for inflation only at room temperature) was 0.457 mm (0.018 in.), which increased to 1.22 mm (0.048 in.) after heating.

Note that from the experimental results, it is evident that there is an f-number change due to the change in center deflection. The experiments conducted here did not consider keeping the f-number constant due to the preliminary nature of the tests. As has been mentioned, by increasing or decreasing the f-number, one can influence the rms error, hence that the results presented in this section may be a combination of heating the surface and f-number change cannot be ruled out.

Conclusions

The work reported here concerns theoretical analysis, FEA, and experimental investigations of shape changes of a precision membrane reflector. The following are some conclusions made through this study.

1) The theoretical, finite element, and experimental approaches to estimating the final shape of an inflated membrane agree within a few percent.

2) Inflated membrane reflectors are formed from initial plane sheets, clamped in circular boundaries, and deformed into doubly curved surfaces. Their profile, when compared to a parabolic shape, demonstrates an aberration, which is caused by the boundary not allowing any motion in the hoop direction. This deviation is seen in the so-called W curve.

3) All three analyses suggest that this surface figure error can be substantially corrected by radial displacements at the boundary.

4) The thermal environment in space can be expected to apply nonuniform heating to the membrane surface, due to partial shading from appendages or other occulting objects. It has been shown that nonuniform surface temperatures have potential to be modeled adequately by FEA.

5) Application of temperature to the reflector may be used to effect changes in the surface profile in desirable or undesirable ways; selective heating of the membrane surface via a laser remains an intriguing possibility.

6) The model was studied for different temperature profiles, varying both in temperature values and spatial extent; both factors are important factors.

7) Even when the thermal loading leads to increased figure errors, boundary displacements can provide significant correction.

Acknowledgments

The authors wish to acknowledge the Air Force Research Laboratory and the Jet Propulsion Laboratory for their support of this work. We also acknowledge that the thermography measurements were supported by InfraTech Systems of Rapid City, South Dakota.

References

[1]Jenkins, C. H., and Marker, D. K., "Surface Precision of Inflatable Membrane Reflectors," *Journal of Solar Energy Engineering*, Vol. 120, 1998, pp. 319–328.

[2]Jenkins, C. H., Kalanovic, V. D., Padmanabhan, K., and Faisal, S. M., "Intelligent Shape Control for Precision Membrane Antennae and Reflectors in Space," *Smart Materials and Structures*, Vol. 8, 1999, pp. 1–11.

[3]Jenkins, C. H., and Leonard, J. W., "Nonlinear Dynamic Response of Membranes: State of the Art," *Appied Mechanics Review*, Vol. 44, 1991, pp. 319–328.

[4]Jenkins, C. H., "Nonlinear Dynamic Response of Membranes: State of the Art-Update," *Applied Mechanics Review*, Vol. 49, No. 10, 1996, pp. S41–S48.

[5]Hencky, H., "Uber den Spannungszustand in Kreisrunden Platten," *Z. Mathematics and Physics*, Vol. 63, 1915, pp. 311–317.

[6]Fichter W. B., "Some Solutions for the Large Deflection of Uniformly Loaded Circular Membranes," NASA TP 3658, 1997.

[7]Wilkes, J. M., "Application of Power Series Solutions of Membrane Equilibrium Equation to The Optical Evaluation of Membrane Mirrors with Curvature," U.S. Air Force Research Lab., AFRL-DE-PS-TR-1998-1069, Kirtland AFB, 1998.

[8]Campbell, J. D., "On the Theory of Initially Tensioned Circular Membranes Subjected to Uniform Pressure," *Quarterly Journal of Mechanics and Applied Mathematics*, Vol. 9, 1956, pp. 84–93.

[9]Faisal, S. M., "Thermoelasticity of Precision Membrane Reflector," M.S. Thesis, Mechanical Engineering Dept., South Dakota School of Mines and Technology, Rapid City, SD, 1998.

[10]Suhir, E., "Failure Criterion for Moisture-Sensitive Plastic Packages of Integrated Circuit Devices: Application of Von-Kármán's Equation with Consideration of Thermoelastic Strains," *International Journal of Solids and Structures*, Vol. 34, No. 23, 1995, pp. 2991–3019.

[11]Jenkins, C. H., Ash, J. A., Wilkes, J. M., and Marker, D. K., "Mechanics of Membrane Mirrors," *Proceedings of the IASS-IACM 2000 Computational Methods for Shell and Spatial Structures*, International Association for Shell and Spatial Structures–International Association for Computational Mechanics, 2000.

H. L. McManus
Associate Editor